Green Chemistry

Cutting-edge research for a greener sustainable future

This article can be cited before page numbers have been issued, to do this please use: M. T. Hoang, N. D. Pham, Y. Yang, V. Tiong, C. Zhang, K. Gui, H. Chen, J. Chang, J. Wang, D. GOLBERG, J. M. Bell and H. Wang, *Green Chem.*, 2020, DOI: 10.1039/D0GC01081B.

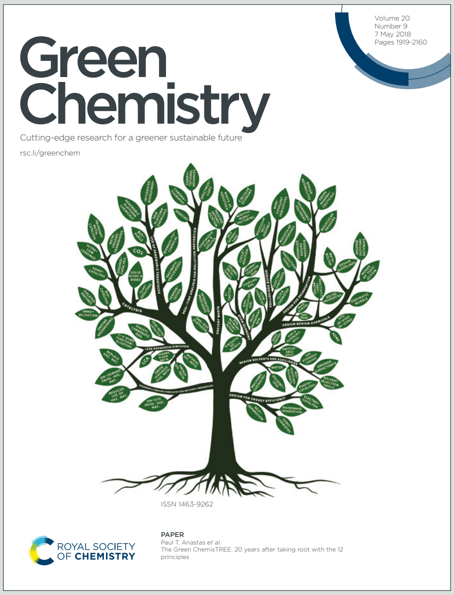

ROYAL SOCIETY OF CHEMISTRY

rsc.li/greenchem

View Article Online
DOI: 10.1039/D0GC01081B

COMMUNICATION

# A facile, environmental-friendly synthesis of strong photo-emissive methylammonium lead bromide perovskite nanocrystals enabled by ionic liquids

Received 00th January 20xx,
Accepted 00th January 20xx

DOI:

Minh Tam Hoang,[a] Ngoc Duy Pham,[a] Yang Yang,[a] Vincent Tiing Tiong,[a] Chao Zhang,[a] Ke Gui,[a] Hong Chen,[b] Jin Chang,[b] Jianpu Wang,[b] Dmitri Golberg,[a] John Bell,[a,c] and Hongxia Wang*[a]

**Herein we demonstrate a new method for synthesis of methylammonium lead bromide perovskite nanocrystals ($MAPbBr_3$) by using environmental-friendly ionic liquids. The effects of different carboxylate anions in the ionic liquids on crystal growth and properties of the $MAPbBr_3$ were investigated. This work paves a new avenue for sustainable synthesis of perovskite materials by using ionic liquid based green solvent.**

In the last decade organo-metallic perovskite materials have attracted enormous attention in the communities of material science and photovoltaics (PV) due to their unprecedented achievement in power conversion efficiency with solar cells, which has increased from 3.2 to 25.2% in ten years with the perovskite material made by solution processing method[1-3]. The outstanding performance of perovskite materials in PV devices is ascribed to their unique optical and electrical properties including composition dependent optimal bandgap, strong light absorption, high defects tolerance, efficient separation of electron-hole pair[4]. Besides PVs, the perovskite has also demonstrated potential in other optoelectronic devices such as light emitting diodes (LEDs), photodetectors and transistors, owing to their strong photo-emissive nature [5, 6]. Compared to thin films based bulk materials, nanocrystal is another important form of a perovskite material owing to the advantageous feature of small particles such as stronger photoemission, size -dependent tuneable band gaps which offer efficient light absorption and luminescence in a broader spectral wavelength ranging from violet to near-infrared[7]. Perovskite nanocrystals (PeNCs) in the form of nanowires or nanoplatelets have demonstrated promising performance for applications such as photodetectors, lasers and other optoelectronic devices [8-10]. LEDs devices made from PeNCs have exhibited exceptional progress with external quantum efficiency reached to 21.3%[11-16].

In all these applications, synthesis of the perovskite materials normally involves extensive use of hazardous solvent. Traditionally thin film perovskite materials are synthesized by wet chemical solution process and PeNCs or QDs can be made by ligand-assisted reprecipitation or hot injection methods which involves the use of noxious solvents like N,N-Dimethylformamide (DMF), Dimethyl sulfoxide (DMSO) or N-methyl-2-pyrrolidone in order to dissolve the lead halide salt precursor [17-21]. These material synthesis methods are not only complex and difficult to control material properties, use of the hazardous solvents are also highly unfavourable in industrial fabrication due to their harmful impact on human health and environment[22]. Furthermore, the highly coordinating solvents (e.g., DMF, DMSO) used in PeNCs synthesis could also lead to degradation of the perovskite NCs by the residual DMF, DMSO solvent in the solution[23]. To address the issues, efforts have been made to develop synthetic process with lower environmentally harmful impact for organo-metal perovskite NCs. For example, less toxic solvent such as acetonitrile (ACN) was used to dissolve $PbI_2$ powder to synthesis methylammonium lead triiodide perovskite nanocrystals. However not only the material synthesis method is complex, the low solubility of the lead salt in ACN and the high vapour pressure of flammable ACN make it challenge for application in large scale material production[24].

Ionic liquids (ILs) are a type of material composed of cations and anions with a melting temperature of less than 100 $^{o}C$. The unique properties of low melting temperature and decent solubility to certain materials have enabled ILs a good choice as a green solvent in material synthesis [25]. The attempts of using ILs based on methylammonium formate (MAF) for synthesis of perovskite thin films were reported. Nevertheless,

---

[a] *School of Chemistry, Physics and Mechanical Engineering, Science and Engineering Faculty, Queensland University of Technology, Brisbane, QLD 4001, Australia. E-mail: hx.wang@qut.edu.au*

[b] *Key Laboratory of Flexible Electronics (KLOFE) & Institute of Advanced Materials (IAM), Nanjing Tech University (NanjingTech), 30 South Puzhu Road, Nanjing 211800, China.*

[c] *Division of Research and Innovation, University of Southern Queensland, PO Box 4393, Raceview, Qld 4305 Australia.*

† Electronic Supplementary Information (ESI) available: [details of any supplementary information available should be included here]. See DOI:

View Article Online
DOI: 10.1039/D0GC01081B

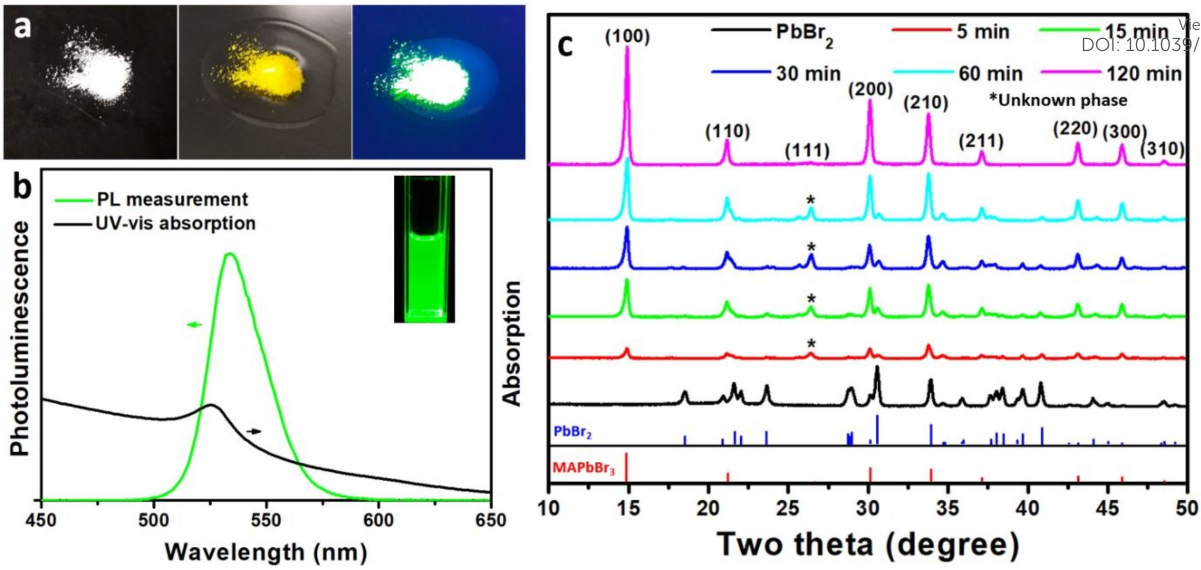

Figure 1: *a) Reaction phenomenon between $PbBr_2$ and MAP; b) UV-vis absorption and photoluminescence spectrum of the product formed by $PbBr_2$ and MAP (inset: dispersion of the sample in toluene under UV-365 nm excitation; c) XRD patterns of the product from reaction between $PbBr_2$ and MAP after different reaction times. The indexed peaks correspond to the perovskite phase. Blue and red bars are standard XRD peak for $PbBr_2$ and $MAPbBr_3$.*

the quality of the synthesized perovskite film was very poor.[26, 27] Most recently methylammonium acetate was used for the production of perovskite films for solar cells, which showed decent performance[28]. To the best of our knowledge, there is no report of synthesis of perovskite nanocrystals using ionic liquids. Herein, we demonstrated the first facile synthesis of highly luminescent $MAPbBr_3$ perovskite nanocrystals by using ionic liquids based on methylammonium carboxylate with different alkyl chains of anions. Highly crystalline $MAPbBr_3$ nanocubes with sizes of 10-20 nm and nanorods with diameter of 80-90 nm were made by controlling carbon chain of anions of the ILs. The synthesized NCs exhibited bright green photoluminescence with narrow full width at half maximum of 28 nm and short radiative lifetime of around 6 ns. This novel method offers a facile, environmental-friendly synthesis pathway for $MAPbBr_3$ NCs with controlled properties for various applications.

A series of methylammonium carboxylate protic ionic liquids with different alkyl chain length were synthesized via reactions of methylamine (Brønsted base) with formic acid, propionic acid and butyric acid (Brønsted acid) to form methylammonium formate (MAF), methylammonium propionate (MAP) and methylammonium butyrate (MAB), respectively. All the materials are liquid at room temperature and are thermally stable with no weight loss until the temperature is more than 90 °C (Figure S1). we have conducted nuclear magnetic resonance (NMR) measurement for the as-synthesized ionic liquids MAF, MAP and MAP. The $^1H$ NMR spectra of the ionic liquid are shown in figure S2. As can be seen, all the detected protons can be assigned to corresponding chemical shift in anion and cation of ionic liquids. The result indicates the successful synthesis of the ILs. When $PbBr_2$ powder is added to the ionic liquid, we found that all the above ionic liquids reacted with $PbBr_2$ instantaneously at room temperature. Figure 1a shows a representative example of a sample formed through the reaction between MAP and $PbBr_2$. The white $PbBr_2$ powder changes to yellow colour immediately in the presence of MAP, which emits strong green light under photoexcitation by a UV lamp (365 nm). The instantaneous change in crystal structure of $PbBr_2$ powder was also revealed by in-situ transmission electron microscopy (TEM) measurement. From the selected area diffraction pattern of $PbBr_2$ powder before and after contact with MAP, we observed the appearance of a new diffraction pattern which can be assigned as the fingerprint of the $MAPbBr_3$ lattice (Figure S3). The yellow powder collected after the reaction can be easily dispersed uniformly into nonpolar solvent like toluene or hexane for further characterisation (Inset in Figure 1b).

The UV-visible absorption spectrum of the dispersion solution (Figure 1b) shows that the material has an absorption peak at ~526 nm corresponding to a band gap of 2.26 eV. A single strong photoemission peak at ~530 nm with narrow FWHM of ~28 nm is observed in photoluminescence (PL) spectrum of the material (Figure 1b). The optical property of the material is consistent with that of $MAPbBr_3$ NCs reported previously[20, 29].

In order to understand the formation mechanism of the perovskite formed by MAP IL with $PbBr_2$, we monitored the evolution of crystal structure of the yellow product at different reaction times by X-ray diffraction (XRD) (Figure 1c). As can be seen, after keeping the $PbBr_2$ powder in MAP liquid for 5 min, new diffraction peaks belonging to cubic $MAPbBr_3$ perovskite appear. The intensity of the $MAPbBr_3$ peaks keeps increasing while intensity of diffraction peaks of $PbBr_2$ decreases with the reaction time. After 2 hours of reaction time, only $MAPbBr_3$ phase was detected with the primary diffraction peaks at 14.93°, 30.12° and 33.79° corresponding to (100), (200) and (210) planes of cubic $MAPbBr_3$ perovskite. We fitted the XRD

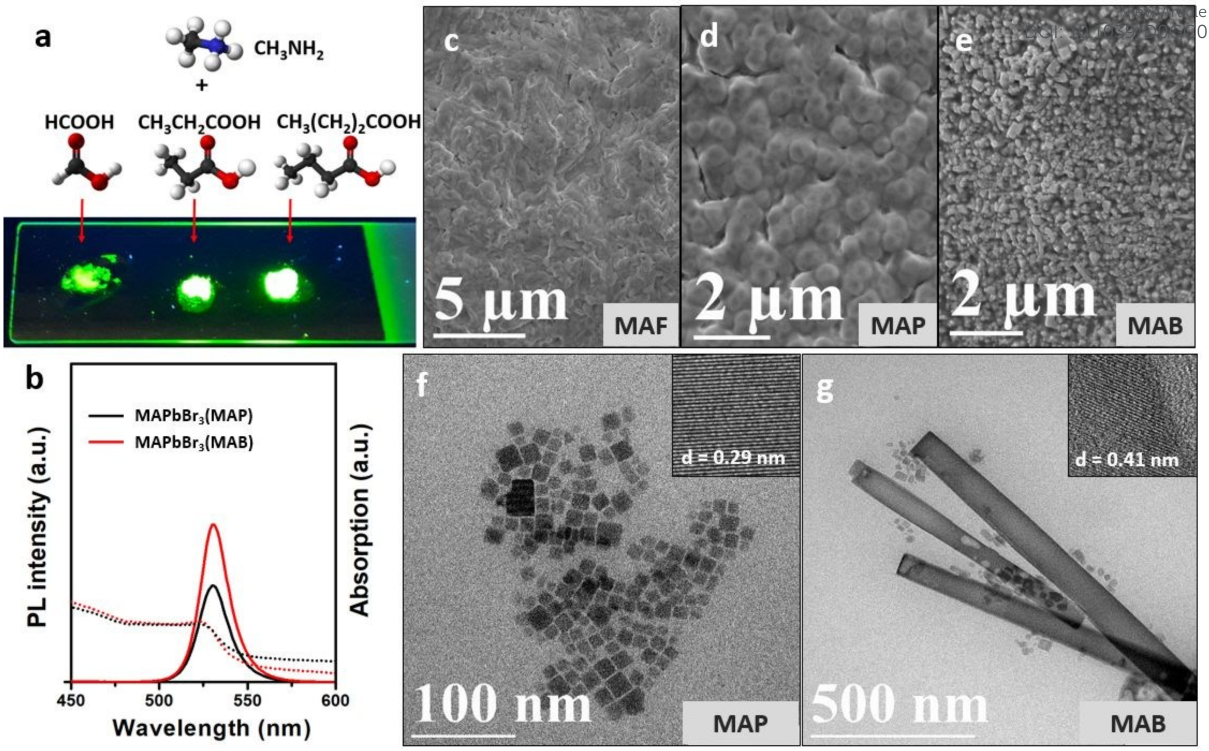

*Figure 2 a) Illustration depicting the reaction of $PbBr_2$ with MAF, MAP and MAB. The product powder shows green emission under UV-365 nm excitation; b) Comparison in PL spectrum of $MAPbBr_3$(MAP) and $MAPbBr_3$(MAB) NCs dispersed in toluene; c-e) SEM images of $MAPbBr_3$(MAF), $MAPbBr_3$(MAP) and $MAPbBr_3$(MAB) powder; f) TEM images of $MAPbBr_3$(MAP) NCs and g) $MAPbBr_3$(MAB) nanorods (Insets in f and g: high resolution TEM image showing the lattice images of corresponding nanocrystals).*

patterns of the material collected at different reaction duration by means of the Rietveld refinement method. We used standard $MAPbBr_3$ (PDF-01-084-9476) and $PbBr_2$ (PDF-04-002-0259) phases as reference in the fitting. The results show that the percentage of $MAPbBr_3$ phase in the material was 71.9%, 79.0%, 83.3%, 93.8% and 100% at the reaction duration of 5 min, 15 min, 30 min, 60 min and 120 min, respectively.

Interestingly, during the phase transformation, an XRD peak at 26.01° (labelled as unknown peak in Figure 1c) was detected for the perovskite formed by MAP with a reaction time up to 60 min. After this, the unknown peak gradually decreases and completely disappeared after 2 hrs. This peak is probably associated with formation of an intermediate phase or complex mainly related with cations of the IL during the formation of perovskite crystals, which is often observed in perovskite phase evolution[30]. Similar phase transformation towards formation of $MAPbBr_3$ perovskite was also found with MAF and MAB based ionic liquid in the presence of $PbBr_2$ (Figure S4). The peak position of the intermediate is located at 27.3° for MAF-based reaction and 26.4° for MAB-based reaction, respectively. This implies that the intermediate phase formed from $PbBr_2$ and the ILs is also affected by the anions of the ILs. We suppose that the phase involves $(PbBr_6)^{4-}$ octahedron which is caged and isolated by carboxylate bridges, forming $MAPbBr_{3-x}$ $(F/P/B)_x$ intermediate. Chao et al. reported a similar phenomenon where an intermediate phase was formed by self-assembly of methylammonium acetate (MAAc) with $PbI_2$ during crystallization of $MAPbI_3$ thin film in MAAc ILs solvent[28]. Furthermore Seo et al. confirmed formation of complex $HCOO^-$ -$Pb^{2+}$ when using MAF as additives in the perovskite precursor solution[31]. The intermediate phases did not affect the crystal structure and phase purity of the perovskite film, which is similar to our case. However, it can have significant effect on the nucleation and crystallization of the perovskite material. For example, the intermediate phase between $PbI_2$ and MAAc ILs effectively hampers the reaction between $PbI_2$ and MAI in the solution[32]. Thus, we believe the anions of formate, propionate and butyrate are involved in the intermediate phases, which in turn affects the crystallization kinetics and ultimately the morphology of the synthesized NCs. For clarity, the perovskites formed with the different ionic liquids of MAF, MAP and MAB are named as $MAPbBr_3$(MAF), $MAPbBr_3$(MAP) and $MAPbBr_3$(MAB) respectively in the following to differentiate the different samples.

Since optical property and morphology are critical features of the perovskite materials, we investigated the effect of the ILs with different anions on optical properties and morphology of $MAPbBr_3$ formed by MAF, MAP and MAB. It is worth to note that carbon chain length of the three ILs is MAF<MAP< MAB. As can be seen in Figure 2a, the brightness of green emission of $MAPbBr_3$ products made from the three PILs increases in the sequence MAF <MAP <MAB, which is the same trend with the increased length of the carbon chain. The different brightness

View Article Online
DOI: 10.1039/D0GC01081B

in photoemission of MAP and MAB products is also clearly seen in the PL measurement (Figure 2b), where $MAPbBr_3$(MAB) shows a much stronger PL peak than the $MAPbBr_3$(MAP) when the absorbances of the samples were adjusted to almost the same value. The stronger PL peak is assigned to the higher radiative recombination. It is worth to point out that we were not able to measure PL spectrum of the $MAPbBr_3$(MAF) sample because the $MAPbBr_3$(MAF) solid cannot be dispersed in toluene due to strong agglomeration of the material (more details are shown below). Furthermore, the different carbon chain of anion also affects the stability of the product. We have found that the $MAPbBr_3$(MAF) is slowly dissolved in residual MAF at room temperature due to the presence of N-methylformamide (DMF) and water as a consequence of condensation reaction of methylammonium cation with the formate anion of MAF[26]. The highly coordinating DMF from the condensation reaction can easily dissolve perovskite materials. In contrast, $MAPbBr_3$ from MAP and MAB appears to be much more stable.

The morphology of as-synthesized $MAPbBr_3$ powder made from the different ionic liquids was analysed by a scanning electron microscope (Figure 2c-e). The $MAPbBr_3$(MAF) shows a sticky, compact morphology, while the $MAPbBr_3$(MAP) shows morphology consisting of lots of egg-like small particles. In contrast, the $MAPbBr_3$(MAB) shows distinct morphology composed of small cubic crystals and nanorods. It is known that smaller particles normally benefit the radiative recombination in perovskites NCs[33]. This explains the different brightness of the green photoemission of the $MAPbBr_3$ materials formed by the three ILs where weak luminescence was observed with $MAPbBr_3$(MAF) and the strongest luminescence with $MAPbBr_3$(MAB).

We further investigated the morphology of the $MAPbBr_3$ materials nanocrystals by TEM measurement of dispersion of the as-synthesized solid in toluene. As mentioned before, due to the agglomerate compact material structure, the $MAPbBr_3$(MAF) could not be dispersed in solvents for characterisation by TEM and PL. Therefore, we only obtained the TEM images of the $MAPbBr_3$(MAP) and $MAPbBr_3$(MAB) materials which could be easily dispersed into nonpolar solvent like toluene or hexane. Figure 2f-g shows the TEM images of $MAPbBr_3$(MAP) and $MAPbBr_3$(MAB). Apparently, the $MAPbBr_3$(MAP) nanocrystals possess a cubic shape with a size ranging from 10 to 20 nm. High-resolution TEM reveals a highly ordered crystalline lattice with clear lattice fringes (Figure 2f inset and Figure S5) of 0.29 and 0.41 nm, corresponding to (200) and (110) planes of cubic $MAPbBr_3$ perovskite, respectively. Whilst the $MAPbBr_3$(MAB) exhibits a collection of different shapes of nanocrystals with nanorods as the most dominant shape. The nanorods have length up to 1μm and a diameter of 80-90 nm. Besides, some small cubic nanocrystals with similar shape but larger size compared to the materials of $MAPbBr_3$(MAP) (Figure S6), were also observed in the $MAPbBr_3$(MAB).

In order to understand the formation mechanism for different morphologies of $MAPbBr_3$(MAB) nanocrystals, we measured TEM of $MAPbBr_3$(MAB) that were collected at different reaction times. As shown in Figure S7, the NCs formed in a short reaction time of 1 min exhibit very thin layered structure with rod or rectangle shape with length of around 400 nm and width of 200-250 nm. Nanorods shape embedded inside the thin layered structure with diameter of 40 nm and length of 300 nm can also be clearly seen. It suggests anisotropic growth of $MAPbBr_3$(MAB) at the beginning of the chemical reaction. Theoretically the stable cubic structure of $MAPbBr_3$ means the materials prefers to grow in all direction uniformly. Practically it is a challenge to make $MAPbBr_3$ nanorods. Petrov et al. reported synthesis of $MAPbBr_3$ nanowires through anion-exchange with $MAPbI_3$ nanowires, which is tedious [34]. The anisotropic growth of the $MAPbBr_3$(MAB) nanocrystals in this work is probably related with the butyrate anion which acted as structure-direct ligands by anchoring on the surface of as-synthesized $MAPbBr_3$ as confirmed by the FTIR measurement below. Since the PL peak of the nanocrystals is similar to that of bulk $MAPbBr_3$, implying that the lateral dimension of the nanocrystals does not possess quantum confinement characteristics, which requires the particle size with at least one dimension less than the Bohn radius of $MAPbBr_3$ (3 nm)[35]. Interestingly, as reaction time increases, the $MAPbBr_3$(MAB) material collected after 2 hrs of reaction time predominantly has the nanorod morphology with a width of 80-90 nm and a few hundred nanometres long. When the reaction time is further increased, the nanorods gradually changes to cubic structures, which are similar to $MAPbBr_3$(MAP) but having a larger size of roughly 40-50 nm. The formation of cubic shape nanocrystal with increased reaction time could be assigned to the exfoliation of the pre-formed $MAPbBr_3$ nanorods due to intercalation of ionic molecules, which have been witnessed in the formation of $MAPbBr_3$ nanoplatelets in a previous report[36]. After that, no significant morphology changes were observed with increase of reaction time. We believe the morphology change is related to the anions of MAB. We also investigated the morphology evolution of $MAPbBr_3$(MAP). We found the $MAPbBr_3$(MAP) materials collected at 1 min reaction time possesses nanospheres shape with size of less than 10 nm, which gradually grow to cubic structures of 10-20 nm in size (Figure S8). It suggests $MAPbBr_3$(MAP) adopted an isotropic growth mechanism in the material nucleation and growth process.

The different crystal formation mechanism clearly indicates the influence of the anions of the ILs on the crystal shape. Fundamentally it is a challenge to understand the formation mechanism of perovskite nanocrystals because of their fast nucleation and growth rate [37]. We believe the formation of perovskite NCs with different morphology in this work is related to (1) the intercalation ability of carboxylate ligands; (2) different diffusion dynamic of the ILs; and (3) the different density of the carboxylate ligands on the surface of the as-formed perovskite. The carboxyl group with different alkyl chain have a very different viscosity. The viscosity of MAP is 40% smaller than MAB and MAF's viscosity is only 10% that of MAB (Figure S9). A faster diffusion dynamic of MAP is thus expected, which means the nucleation of the $MAPbBr_3$(MAP) is faster and the anions ligand can quickly leave the surface

View Article Online
DOI: 10.1039/D0GC01081B

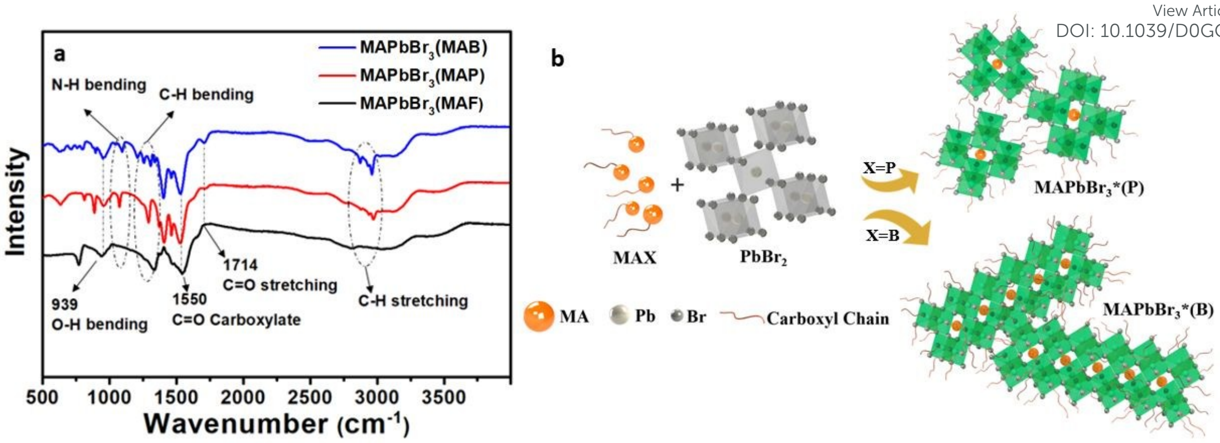

Figure 3: *a) FTIR spectra of MAPbBr$_3$ NCs prepared while using different ionic liquids; b) illustration of reaction scheme between ionic liquid MAX with tetragonal PbBr$_2$ to form MAPbBr$_3$ nanocubes and nanorods crystals where X is acting as surface ligands.*

compared to MAB, which thus favours an isotropic growth. When high concentration of large anion such as butyrate anchors on the as-formed MAPbBr$_3$ nanocrystals, the material can follow anisotropic growth[38]. In additional, ionicity is an important factor of ILs, which can influence the PeNCs synthesis. Ionicity can be quantified as the effective fraction of ions available to participate in conduction[39]. To compare the ionicity of the MAF, MAP and MAB, considering that having shorter alkyl chain can lead to lower viscosity and higher ionicity[40], and the odds number of carbon chain tends to have a higher ionicity than expected comparing to the even number of carbon presented[25], we expected that the ionicity follows MAF > MAP > MAB. It is possible that the higher ionicity of MAP offers a more rapid crystallization compared to MAB. Furthermore the ionicity of IL can also affect the surface stabilization and aggregation of nanoparticles through influence the layer of anionic species at the surface of particles or formation of ionic aggregates close to the surface [41-43]. Ionicity have strong correlation with conventional solvent parameters like polarity, conductivity, viscosity and surface tension, thus, the effect of ionicity can also described through those conventional parameters. For example, ionicity can be evaluated from polarity, which is greatly contributed from dipole moment of dissociated anions in ILs[44]. On the other hand, the dipole moment indicates the affinity of anion toward reactants such as Pb$^{2+}$ ion, which trigger the phase transformation. Overall, ionicity can be a useful indicator to characterize the ability of ILs in the PeNCs synthesis and the effect of which will require further study.

In order to confirm the existence of different density of carboxyl ligands on the surface of the perovskite nanocrystals made from the ILs with different anions, we recorded Fourier-transform infrared spectra (FTIR) of the synthesized perovskite. As shown in Figure 3a, the observed vibration peaks of O–H (939 cm$^{-1}$) and C=O (1714 cm$^{-1}$, 1550 cm$^{-1}$) indicate existence of carboxylate groups on the surface of all three perovskite materials. At a higher wavenumber region, a broad peak in the range of 2500 – 3300 cm$^{-1}$ matches the characteristic C–H stretching, which is characteristic of the hydrogen-bonded O–H group of carboxylic acid[45]. These observations imply that the carbon chain in the carbonyl group is indeed attached onto the surface of the perovskite NCs after the fast reaction.

Based on the FTIR spectrum of these three samples, we have also found that the intensity of the vibration peaks of the surfactants in the N–H, C–H bending and C–H stretching region follows the order of MAPbBr$_3$(MAB)> MAPbBr$_3$(MAP)> MAPbBr$_3$(MAF). The distinct vibration peak of the surfactant is the strongest in MAPbBr$_3$(MAB), while these fingerprint peaks almost disappear in MAPbBr$_3$(MAF), suggesting different density of the ligands on the material surface. This low surfactant density can result in agglomeration of the synthesized NCs and increased surface traps on the NCs, which ultimately leads to poor optical properties of the nanocrystal material[46]. This explains the different dispersion ability of the perovskite in solvent and their different photoemission property. Furthermore, the highest density of long chain butyrate anion of MAB means some facet of the perovskite nanocrystals was densely protected by the anion ligand from growth, leading to anisotropic grow of the nanocrystals and formation of nanorods. While the mild density and shorter chain of propionate ligand of MAP did not provide enough impact to induce anisotropic growth of the materials. Clearly the surface ligands in this work act as several beneficial roles including (1) prevention of aggregation of the NCs; (2) act as structure-direct agent for growth of the MAPbBr$_3$ and (3) passivation of surface defects of the NCs, just similar to the role of Oleic acid which is widely used in PeNCs synthesis[47]. However, compared to the long chain oleate (18 carbon chain) that is extensively used in PeNCs synthesis, our work shows that shorter chain carboxylate (three (MAP) or four carbon chain (MAB)) can also work as an effective surface ligand for growth of perovskite nanocrystals. An additional advantage of the shorter chain carboxyl ligands is that they are more desirable for charge transfer in semiconductor materials compared to insulating nature of long chain ligands. [46, 48]

View Article Online
DOI: 10.1039/D0GC01081B

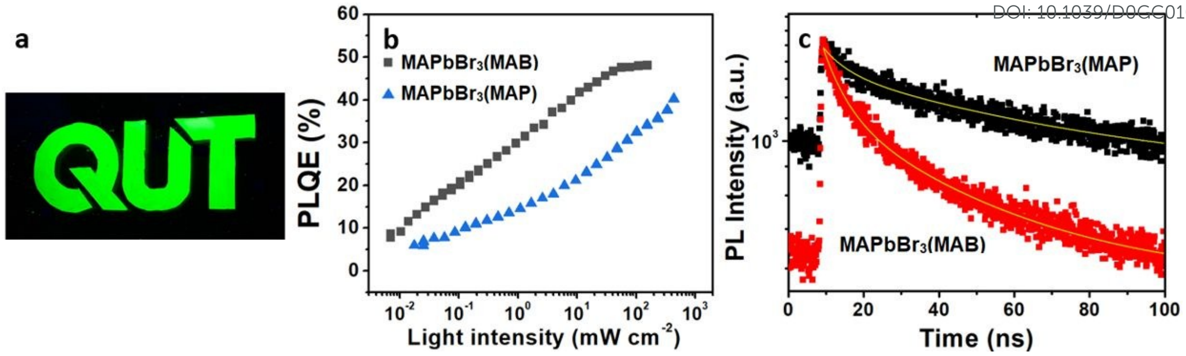

Figure 4: a) Printing pattern made from $MAPbBr_3$(MAB) NCs showing strong green emission under UV-365 nm excitation; b) excitation-intensity-dependent photoluminescence quantum efficiencies of thin films fabricated from $MAPbBr_3$(MAP) and $MAPbBr_3$(MAB) ink; c) TR-PL spectrum $MAPbBr_3$(MAP) and $MAPbBr_3$(MAB).

In order to demonstrate the universal of this synthesis method, we have also used ILs containing longer alkyl chains made from valeric acid or from nonlinear chain such as aromatic ring like benzoic acid. The methylammonium valerate (MAV) made from valeric acid is liquid while methylammonium benzoate (MABe) made from benzoic acid is solid at room temperature. However, MABe becomes liquid at around 60 °C. Similar to MAP and MAB, we found both MAV and MABe can react with $PbBr_2$ immediately to form $MAPbBr_3$ NCs, which also showed strong photoemission. It should be noted that the reaction with $PbBr_2$ was conducted at 60°C. The optical properties of $MAPbBr_3$(MAV) and $MAPbBr_3$(MABe) is shown in figure S10a, b. The TEM measurement also reveals cubic perovskite NCs with size up to 30nm for $MAPbBr_3$(MAV) while nanocrystals of $MAPbBr_3$(MABe) have much smaller sizes (10 nm) with irregular shape (figure S10c, d). FTIR measurement also was conducted to confirm the presence of carboxylate ligand on surfaces of the NCs (Figure S11).The synthesized NCs is similar to $MAPbBr_3$ NCs synthesized by using benzylamine and benzoic acid as capping ligands as reported previously [49]. These results indicate the universal of this ionic liquid based green solvent method for synthesis of $MAPbBr_3$ NCs. They also clearly show the effect of different anions on tuning the size and shape of the perovskite nanocrystals. The underlying mechanism controlling the formation and growth of perovskite NCs by MAV and MABe will be investigated in the future.

To test the performance of the $MAPbBr_3$ nanocrystals formed by MAP and MAB, we made perovskite thin films using an ink incorporating the $MAPbBr_3$(MAB) NCs perovskite NCs by doctor blading (Figure 4a, Figure S12 a, b). SEM shows compact, uniform morphology of the film (Figure S12c). As shown in Figure 4a, a patterned perovskite film made from the as-synthesized $MAPbBr_3$(MAB) NCs exhibits strong luminescence under UV excitation (365 nm). It is notable that, the photoluminescence quantum efficiency (PLQE) of $MAPbBr_3$(MAB) is much higher than that of $MAPbBr_3$(MAP), suggesting that $MAPbBr_3$(MAB) possesses less trap density, which is probably related with the smaller crystal sizes and the higher density of the carboxyl ligands on the materials surface. At high light intensity of ~100 mW cm$^{-2}$, the PLQE is ~50% for $MAPbBr_3$(MAB) and ~40% for $MAPbBr_3$(MAP) which is comparable to the materials made by using other solvents reported in literature (Table S1). The excitation-intensity-induced increase of PLQE is mainly attributed to the defect filling process under illumination. The time-resolved photoluminescence (TR-PL) spectrum of the thin film, fitted with a biexponential function, shows a very short lifetime of the NCs. The short-lived ($\tau_1$) and long-lived ($\tau_2$) components of the luminescence decay are 6.02 ns and 42.29 ns for $MAPbBr_3$(MAB), 6.04 ns and 73.38 ns for $MAPbBr_3$(MAP) respectively. The detail fitting data are listed in table S2. The short-lifetime is originated from exciton radiative recombination, which indicates that both materials have effective radiative recombination compared to PeNCs made by using other methods[24, 50]. The longer PL lifetime ($\tau_2$) is associated with longer charge trap/detrapping process. The longer $\tau_2$ of $MAPbBr_3$(MAP) compared to $MAPbBr_3$(MAB) is consistent with its higher surface defects due to lower density of surface ligands according to the FTIR results and the PLQE measurement. Interestingly, the film was even stable in water. There was no observable degradation after the material was immersed in water for one hour (Figure S13). This is probably due to the hydrophobic nature of the alkyl chains on the surface of PeNCs.

Furthermore, the ionic liquid based green synthesis method has good reproducibility and is suitable for large scale fabrication of $MAPbBr_3$ NCs. We scaled-up the synthesis of $MAPbBr_3$ NCs method by using 1g of $PbBr_2$ precursor with MAB (MAP), which produced 425.5 mg (348.6 mg) of $MAPbBr_3$ NCs in one batch. The obtained NCs exhibit high purity and good optical properties to the material made at small scale as shown in Figure S14).

## Conclusions

In conclusion, we have demonstrated a benign method to synthesize green emissive $MAPbBr_3$ PeNCs by using an environmentally friendly solvent based on ionic liquids. The perovskite NCs with controlled sizes and shapes (nanocubes, nanorods) and subsequently high photoluminescence have

View Article Online
DOI: 10.1039/D0GC01081B

been obtained by controlling the alkyl chain length of the carboxylate group and reaction time. Compared to other synthesis method of PeNCs, our method has the advantages of facile processing and is environmentally friendly. These two merits are highly desirable and important for the large-scale production of perovskites. Therefore, the demonstrated facile, green material synthesis method paves a new way towards sustainable industrial production of perovskite materials for variable applications.

## Conflicts of interest

The authors declare no conflict of interest.

## Acknowledgements

This work was supported by Australian Research Council Discovery Project (DP190102252) and Centre for Materials Science at Queensland University of Technology (QUT). M.T. H. QUT postgraduate scholarship. The data of SEM, TEM, fluorescence reported in this paper were obtained at the Central Analytical Research facility (CARF), QUT. Access to CARF was supported by the generous funding from Science and Engineering faculty, QUT. A great thank to Dr. Peng Chen, University of Queensland, for the TR-PL measurement. C.Z and D.G are grateful to the ARC Laureate project FL160100089 for funding.

## Notes and references

1. NREL, https://www.nrel.gov/pv/assets/pdfs/best-research-cell-efficiencies.20190802.pdf.
2. A. Kojima, K. Teshima, T. Miyasaka and Y. Shirai, 2006, 397
3. Q. Jiang, Y. Zhao, X. Zhang, X. Yang, Y. Chen, Z. Chu, Q. Ye, X. Li, Z. Yin and J. You, *Nat. Photonics*, 2019, **13**, 460-466.
4. M. A. Green, A. Ho-Baillie and H. J. Snaith, *Nat. Photonics*, 2014, **8**, Nat. photonics, 2014, 8, 506-514.
5. J. S. Manser, J. A. Christians and P. V. Kamat, *Chem. Rev.*, 2016, **116**, 12956-13008.
6. Q. A. Akkerman, G. Rainò, M. V. Kovalenko and L. Manna, *Nat. Mater.*, 22018, **17**, 394-405.
7. L. Protesescu, S. Yakunin, M. I. Bodnarchuk, F. Krieg, R. Caputo, C. H. Hendon, R. X. Yang, A. Walsh and M. V. Kovalenko, *Nano Lett.*, 2015, **15**, 3692-3696.
8. Y. Meng, C. Lan, F. Li, S. Yip, R. Wei, X. Kang, X. Bu, R. Dong, H. Zhang and J. C. Ho, *ACS nano*, 2019, **13**, 6060-6070.
9. Q. Zhou, J. G. Park, R. Nie, A. K. Thokchom, D. Ha, J. Pan, S. I. Seok and T. Kim, *ACS nano*, 2018, **12**, 8406-8414.
10. M. C. Weidman, A. J. Goodman and W. A. Tisdale, *Chem. Mater.*, 2017, **29**, 5019-5030.
11. H. Liu, Z. Wu, J. Shao, D. Yao, H. Gao, Y. Liu, W. Yu, H. Zhang and B. Yang, *ACS nano*, 2017, **11**, 2239-2247.
12. X. Du, G. Wu, J. Cheng, H. Dang, K. Ma, Y.-W. Zhang, P.-F. Tan and S. Chen, *RSC Advances*, 2017, **7**, 10391-10396.
13. Y. Chang, Y. J. Yoon, G. Li, E. Xu, S. Yu, C.-H. Lu, Z. Wang, Y. He, C. H. Lin and B. K. Wagner, *ACS Appl. Mater. Interfaces*, 2018, **10**, 37267-37276.
14. D. Liang, Y. Peng, Y. Fu, M. J. Shearer, J. Zhang, J. Zhai, Y. Zhang, R. J. Hamers, T. L. Andrew and S. Jin, *ACS nano*, 2016, **10**, 6897-6904.
15. Y. Liu, J. Cui, K. Du, H. Tian, Z. He, Q. Zhou, Z. Yang, Y. Deng, D. Chen and X. Zuo, *Nat. Photonics*, 2019, **13**, 760-764.
16. T. Chiba, Y. Hayashi, H. Ebe, K. Hoshi, J. Sato, S. Sato, Y.-J. Pu, S. Ohisa and J. Kido, *Nat. Photonics*, 2018, **12**, 681.
17. C. Geng, S. Xu, H. Zhong, A. L. Rogach and W. Bi, *Angew. Chem.*, 2018, **57**, 9650-9654.
18. T. C. Jellicoe, J. M. Richter, H. F. Glass, M. Tabachnyk, R. Brady, S. n. E. Dutton, A. Rao, R. H. Friend, D. Credgington and N. C. Greenham, *J. Am. Chem. Soc.*, 2016, **138**, 2941-2944.
19. J. Shamsi, A. S. Urban, M. Imran, L. De Trizio and L. Manna, *Chem. Rev.*, 2019, **119**, 3296-3348.
20. L. C. Schmidt, A. Pertegás, S. González-Carrero, O. Malinkiewicz, S. Agouram, G. Mínguez Espallargas, H. J. Bolink, R. E. Galian and J. Pérez-Prieto, *J. Am. Chem. Soc.*, 2014, **136**, 850-853.
21. F. Zhang, H. Zhong, C. Chen, X.-g. Wu, X. Hu, H. Huang, J. Han, B. Zou and Y. Dong, *ACS nano*, 2015, **9**, 4533-4542.
22. T. H. Kim and S. G. Kim, *Saf. Health Work*, 2011, **2**, 97-104.
23. F. Zhang, S. Huang, P. Wang, X. Chen, S. Zhao, Y. Dong and H. Zhong, *Chem. Mater.*, 2017, **29**, 3793-3799.
24. Y. Hassan, O. J. Ashton, J. H. Park, G. Li, N. Sakai, B. Wenger, A.-A. Haghighirad, N. K. Noel, M. H. Song and B. R. Lee, *J. Am. Chem. Soc.*, 2019, **141**, 1269-1279.
25. T. L. Greaves and C. J. Drummond, *Chem. Rev.*, 2015, **115**, 11379-11448.
26. S. Öz, J. Burschka, E. Jung, R. Bhattacharjee, T. Fischer, A. Mettenbörger, H. Wang and S. Mathur, *Nano Energy*, 2018, **51**, 632-638.
27. D. T. Moore, K. W. Tan, H. Sai, K. P. Barteau, U. Wiesner and L. A. Estroff, *Chem. Mater.*, 2015, **27**, 3197-3199.
28. L. Chao, Y. Xia, B. Li, G. Xing, Y. Chen and W. Huang, *Chem*, 2019, **5**, 995-1006.
29. H. Huang, A. S. Susha, S. V. Kershaw, T. F. Hung and A. L. Rogach, *Adv. Sci.*, 2015, **2**, 1500194.
30. S. Sanchez, U. Steiner and X. Hua, *Chem. Mater.*, 2019, **31**, 3498-3506.
31. J. Y. Seo, T. Matsui, J. Luo, J. P. Correa-Baena, F. Giordano, M. Saliba, K. Schenk, A. Ummadisingu, K. Domanski and M. Hadadian, *Adv. Energy Mater.*, 2016, **6**, 1600767.
32. Y. Xia, C. Ran, Y. Chen, Q. Li, N. Jiang, C. Li, Y. Pan, T. Li, J. Wang and W. Huang, *J. Mater. Chem. A*, 2017, **5**, 3193-3202.
33. L. Polavarapu, B. Nickel, J. Feldmann and A. S. Urban, *Adv. Energy Mater.*, 2017, **7**, 1700267.
34. A. A. Petrov, N. Pellet, J.-Y. Seo, N. A. Belich, D. Y. Kovalev, A. V. Shevelkov, E. A. Goodilin, S. M. Zakeeruddin, A. B. Tarasov and M. Graetzel, *Chem. Mater.*, 2016, **29**, 587-594.
35. J. A. Sichert, Y. Tong, N. Mutz, M. Vollmer, S. Fischer, K. Z. Milowska, R. García Cortadella, B. Nickel, C. Cardenas-Daw and J. K. Stolarczyk, *Nano Lett.*, 2015, **15**, 6521-6527.
36. Y. Tong, F. Ehrat, W. Vanderlinden, C. Cardenas-Daw, J. K. Stolarczyk, L. Polavarapu and A. S. Urban, *ACS nano*, 2016, **10**, 10936-10944.
37. T. Udayabhaskararao, M. Kazes, L. Houben, H. Lin and D. Oron, *Chem. Mater.*, 2017, **29**, 1302-1308.

View Article Online
DOI: 10.1039/D0GC01081B

38. V. I. Klimov, *Semiconductor and metal nanocrystals: synthesis and electronic and optical properties*, CRC Press, 2003.
39. D. R. MacFarlane, M. Forsyth, E. I. Izgorodina, A. P. Abbott, G. Annat and K. Fraser, *Phys. Chem. Chem. Phys*, 2009, **11**, 4962-4967.
40. T. Yasuda, H. Kinoshita, M. S. Miran, S. Tsuzuki and M. Watanabe, *J. Chem. Eng. Data*, 2013, **58**, 2724-2732.
41. J. Dupont and J. D. Scholten, *Chem. Soc. Rev.*, 2010, **39**, 1780-1804.
42. S. Özkar and R. G. Finke, *J. Am. Chem. Soc.*, 2002, **124**, 5796-5810.
43. K. L. Luska and A. Moores, *Green Chem.*, 2012, **14**, 1736-1742.
44. K. Ueno, H. Tokuda and M. Watanabe, *Phys. Chem. Chem. Phys*, 2010, **12**, 1649-1658.
45. J. Coates, *Encyclopedia of analytical chemistry: applications, theory and instrumentation*, 2006.
46. J. Li, L. Xu, T. Wang, J. Song, J. Chen, J. Xue, Y. Dong, B. Cai, Q. Shan and B. Han, *Adv. Mater.*, 2017, **29**, 1603885.
47. H. Huang, J. Raith, S. V. Kershaw, S. Kalytchuk, O. Tomanec, L. Jing, A. S. Susha, R. Zboril and A. L. Rogach, *Nat. Commun.*, 2017, **8**, 996.
48. H. Huang, M. I. Bodnarchuk, S. V. Kershaw, M. V. Kovalenko and A. L. Rogach, *ACS Energy Lett.*, 2017, **2**, 2071-2083.
49. E. T. Vickers, T. A. Graham, A. H. Chowdhury, B. Bahrami, B. W. Dreskin, S. Lindley, S. B. Naghadeh, Q. Qiao and J. Z. J. A. E. L. Zhang, *ACS Energy Lett.*, 2018, **3**, 2931-2939.
50. S. Sun, D. Yuan, Y. Xu, A. Wang and Z. Deng, *ACS nano*, 2016, **10**, 3648-3657.